Significance of conservative asparagine residues in the thermal hysteresis activity of carrot antifreeze protein

Dang-Quan ZHANG, Bing LIU, Dong-Ru FENG, Yan-Ming HE, Shu-Qi WANG, Hong-Bin WANG and Jin-Fa WANG[1]

The Key Laboratory of Gene Engineering of Ministry of Education, School of Life Sciences, Sun Yat-sen University, Guangzhou 510275, China

The ~24-amino-acid leucine-rich tandem repeat motif (PXXXXXLXXLXXLXLSXNXLXGXI) of carrot antifreeze protein comprises most of the processed protein and should contribute at least partly to the ice-binding site. Structural predictions using publicly available online sources indicated that the theoretical three-dimensional model of this plant protein includes a 10-loop β-helix containing the ~24-amino-acid tandem repeat. This theoretical model indicated that conservative asparagine residues create putative ice-binding sites with surface complementarity to the 1010 prism plane of ice. We used site-specific mutagenesis to test the importance of these residues, and observed a distinct loss of thermal hysteresis activity when conservative asparagines were replaced with valine or glutamine, whereas a large increase in thermal hysteresis was observed when phenylalanine or threonine residues were replaced with asparagine, putatively resulting in the formation of an ice-binding site. These results confirmed that the ice-binding site of carrot antifreeze protein consists of conservative asparagine residues in each β-loop. We also found that its thermal hysteresis activity is directly correlated with the length of its asparagine-rich binding site, and hence with the size of its ice-binding face.

Key words: antifreeze protein, ice-binding site, leucine-rich repeat, structure prediction, thermal hysteresis.

INTRODUCTION

AFPs (antifreeze proteins) can effectively protect organisms from damage during freezing conditions by a process termed TH (thermal hysteresis), i.e. the presence of a hysteresis gap, which is the lowering of the freezing point non-colligatively while leaving the melting point unchanged. The TH activities of AFPs found in fish, insects, plants and bacteria display distinct differences. Plant AFPs have been identified in species such as bittersweet nightshade (*Solanum dulcamara*) [1], winter rye (*Secale cereale*) [2], carrot (*Daucus carota*) [3] and ryegrass (*Lolium perenne*) [4]. They have a relatively weak TH activity of ~0.1–0.5 °C, which is less than that of fish AFPs and significantly less than that of insect AFPs. Great progress has been made in understanding the ice-binding mechanism of fish [5–8] and insect [9,10] AFPs, including a full interpretation of their tertiary structures. In contrast, little is known regarding protein structures of plant AFPs, except for a single theoretical model of that from ryegrass [11].

Despite numerous structural and functional studies on AFPs, their molecular ice-binding mechanism remains poorly understood. Although it is known that AFPs act through adsorption to the ice surface [12,13], the relative contributions of various physical forces to ice binding has not been completely established. However, binding to an AFP should be almost irreversible, because any significant off-rate would lead to ice growth [14]. Progress in understanding the mechanism of binding between ice crystals and fish and insect AFPs has been expedited based on their solved structures [5–10]. Recent research on insect AFPs has shown that the rigid hydrophobic binding site consists of conservative threonine residues that are required for ice binding [15], and that TH activity is directly correlated with the length of the AFP's β-helical structure, i.e. the size of its ice-binding face [16]. The TH activity of fish AFPs relies heavily on hydrophobic and van der Waals interactions, with hydrogen bonding playing a secondary role in the AFP-induced inhibition of ice growth [17,18]. In addition, dimerization of fish AFP has implications for its effective solution concentration and the measurement of its activity [19]. However, the underlying ice-binding mechanism in fish and insect AFPs is similar, in that both rely on close surface complementarity between the AFP and the ice crystal [20,21]. It is assumed that this general mechanism may be applicable to plant AFPs as well.

We have been investigating DcAFP (carrot AFP) since it was identified and isolated [22,23], and have obtained an AFP gene from a Chinese carrot cultivar that has three base changes (one amino acid change) compared with the sequence published in GenBank [24]. The strong antifreeze activity of transgenic tobacco expressing an exogenous form of this gene product indicated that it has ice RI (recrystallization inhibition) activity, which could be confirmed by the method of 'splat cooling' [25]. However, the TH activity of recombinant proteins from an *Escherichia coli* expression system is weak, as is that of the protein *in vivo*. The discordance between the RI and the TH of DcAFP is also observed for other plant AFPs [26], although it is not well understood. Thus AFPs have the general characteristics of TH and RI [27], but plant AFPs have a greater effect on RI than on TH [4].

In a first effort towards understanding the mechanism of binding between ice and plant AFPs, we have examined the predicted three-dimensional structure of DcAFP and attempted to characterize the sequence–function relationships of the protein. Here we report the discovery of putative ice-binding sites with surface complementarity to the 1010 prism plane of ice, as well as the identification of amino acids that play key roles in the binding of DcAFP to the surface of ice.

Abbreviations used: AFGP, antifreeze glycoprotein; AFP, antifreeze protein; DcAFP, carrot (*Daucus carota*) antifreeze protein; LRR, leucine-rich repeat; PGIP, polygalacturonase inhibitor protein; PvPGIP, *Phaseolus vulgaris* PGIP; RI, recrystallization inhibition; TH, thermal hysteresis.

[1] To whom correspondence should be addressed (e-mail Ls19@zsu.edu.cn).

Figure 1 New alignment of the amino acid sequence of mature DcAFP

The 24-amino-acid LRR motif of DcAFP is shaded, conservative asparagine residues are boxed, and strongly hydrophilic amino acids flanking conservative asparagines are underlined. The sequence prior to Ile-278, condensed or expanded at three different positions for an optimal alignment of the consensus sequence, was as aligned as in [19], while the sequence beyond Pro-279 is newly aligned according to our analytical results with the signal sequence removed.

EXPERIMENTAL

Structural predictions

Protein structure predictions were carried out via the MetaServer interface [28] using publicly available online services for folding recognition, including SUPERFAMILY [29], FFAS [30], 3D-PSSM [31], BIOINBGU [32], Genthreader [33], SAM-T99 [34], FUGUE [35], Geno3D [36] and 3D-Jigsaw [37], as well as programs for secondary structure prediction, including JPRED2 [38], PHD [39], PREDATOR [40] and PSI-PRED [41]. The results were evaluated by the Pcons consensus server [42], which compares the models and associated scores to produce a ranking of target–template alignments in comparison with related proteins with known structures. The consensus alignments provided by MetaServer served as a basis for homology modelling carried out using the SWISS-MODEL/PROMOD II server [43]. Protein structure evaluation was carried out using the Verify3D program [44]; this evaluation indicated that the stereochemistry and energetic parameters of the model are acceptable.

Protein structure analysis

Protein Explorer [45] was used for all protein structure manipulations, calculations of conservation scores and electrostatic potential distribution, and generation of the Figures. Protein surface docking was carried out using program 3D-DOCK [46].

Site-directed mutagenesis

On the basis of protein structure prediction and structural analysis of DcAFP, site-directed mutagenesis of potentially important conservative asparagine residues was carried out by overlap extension PCR [47] to create valine mutageneses and steric glutamine replacements of conservative asparagines. In addition, mutagenesis of Glu-57, Pro-82 and Thr-106 to asparagines was carried out. All mutations were confirmed by DNA sequencing.

Fluorescence spectroscopy

The measurement of fluorescence was used to confirm possible conformational differences between wild-type DcAFP and its mutants. Protein concentration was determined with the BCA protein assay kit (Pierce). A 0.1 mg sample of protein in 1 ml of 50 mM Tris/HCl buffer (pH 8.0) was excited at 280 nm. The emission spectra were recorded between 300 and 500 nm using an F-4500 spectrofluorimeter (Hitachi).

Protein expression and purification

The following general conditions were used for all protein preparations. Expression system BL21(DE3)/pET-11a (Novagen) was used for expression of wild-type DcAFP and its mutants in *E. coli* [48]. The primary expression products were processed by ultrasonication and washing, after which they were purified and refolded using the method described by Burgess [49]. A protein solution concentrated by ultrafiltration on Macrosep centrifugal devices (PALL) was finally purified using the simple and convenient method as described by Zhang et al. [50]. Protein purity was checked by SDS/PAGE, and protein concentration was determined with the BCA protein assay kit (Pierce).

Measurement of TH activity

Purified recombinant proteins were used for measurement of TH activity using a nanolitre osmometer (Clifton Technical Physics, Hartford, CT, U.S.A.), essentially following the procedure of Chakrabartty and Hew [51]. TH is defined as the difference between the melting point and the non-equilibrium freezing point of a solution. This was determined by slowly cooling a drop of AFP solution that contained a small ice crystal until the ice grew. In order to improve the accuracy and consistency of measuring small differences in TH, all seed crystals were manipulated by another cycle of freezing and melting at a very low rate in order to attain a very small crystal before measuring the freezing temperature.

RESULTS

Structural predictions

DcAFP contains a series of tandem LRRs (leucine-rich repeats) consisting of ~24 (23–25) amino acids with the motif PXXXXX-LXXLXXLXLSXNXLXGXI. A previously published alignment of DcAFP indicated that the portion of the protein beyond Pro-279 did not correspond to the LRR motif [22]. However, our alignment using current techniques showed that the fragment does show characteristics of a LLR motif (Figure 1). This result was very important to later homology modelling, as the accuracy of such modelling is reduced if amino acid sequences are irregular at both ends. Hence the new alignment of the sequence beyond Pro-279 should increase the accuracy and credibility of our homology modelling.

The sequence of DcAFP was analysed using the structure prediction program MetaServer, which provided compelling evidence that this protein is related to members of the LRR

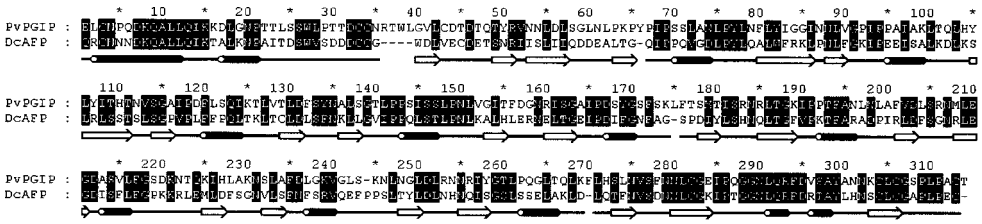

Figure 2 Alignment of the structural templates of PvPGIP and DcAFP

Identical residues are highlighted. Predicted secondary structure elements of DcAFP are shown as cylinders (helices) and arrows (β-sheets). A regular structural arrangement, 'sheet-sheet-helix', just lying in the 24-amino-acid LRR motif, characterizes the fold of the central LRR domain (residues 48–286).

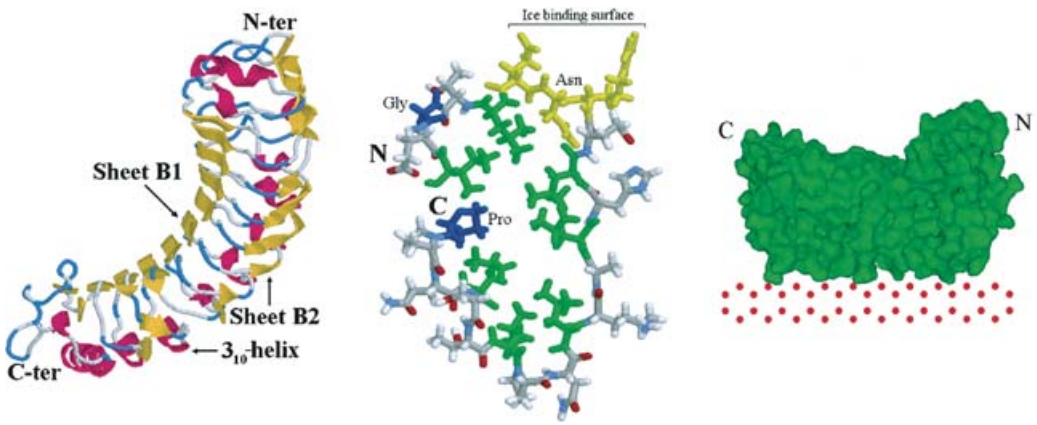

Figure 3 Theoretical structure and ice-binding sites of DcAFP

Left panel: three-dimensional structure of DcAFP, with two β-sheets and a 3_{10}-helix in each β-loop. Sheets B1 and B2 are depicted in yellow, helices are red, and β-turns are blue. Putative ice-binding sites lie between two β-sheet rolls, not inside any single β-sheet roll as is seen in insect and ryegrass AFPs. Middle panel: cross-section of the DcAFP model, showing positions of conservative residues of the LRR motif and the putative ice-binding surface. The conserved internal leucine residues (including isoleucine), which are depicted in green, form a leucine stack along the centre of the β-roll. The presence of a large number of leucine residues in these leucine stacks will lead to the formation of a strongly hydrophobic core at the centre of the β-roll, thus stabilizing the fold of DcAFP. The conserved glycine and proline residues (dark blue) occur at the turns, allowing the β-sheets to bend into the β-roll. Right panel: surface–surface complementarity between DcAFP and ice. The molecular surface of DcAFP (green) can be docked to the 1010 prism plane of ice. Ice oxygen atoms are represented by red dots. Each successive loop matches the 4.5 Å repeat spacing of the ice along the prism face.

superfamily. Most of the individual fold recognition servers detected similarity between DcAFP and the LRR fold. The Pcons consensus server evaluated this prediction as highly confident. In order to characterize the sequence–function relationships of DcAFP at the structural level, we built and evaluated a three-dimensional model. The crystal structure of PvPGIP (the polygalacturonase inhibitor protein of *Phaseolus vulgaris*; PDB ID 1OGQ [52]) was used as the template, since it was the top match found by the Pcons consensus server (Pcons score = 3.71) between LRR proteins with a solved structure and DcAFP (Figure 2). The quality of the theoretical model of DcAFP was evaluated as reasonable (average Verify3D score = 0.28); hence we used it to identify the putative ice-binding sites.

Analysis of protein structure of DcAFP, and implications for the ice-binding mechanism

The central domain in the theoretical model of DcAFP displays a regular β-helix structure consisting of a set of 10 tandemly repeating units, each made up of two β-sheets and a short 3_{10}-helix in each loop of $\sim$24 (23–25) residues in the LRR motif (Figure 3, left panel). The fold is supported by a conservative leucine (including isoleucine) hydrophobic core and conservative β-turns of glycine and proline. The hydrophobic core is formed by the orientation of side chains of leucine and isoleucine residues

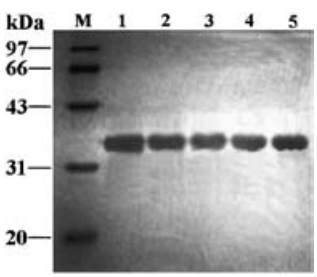

Figure 4 SDS/PAGE of purified recombinant wild-type and mutant DcAFP proteins

Lane M, molecular mass markers; lane 1, purified recombinant wild-type DcAFP; lane 2–4, mutant proteins N130V, N130Q and T106N respectively; lane 5, multi-site mutant E57N/P82N/T106N.

(occasionally substituted by phenylalanine, tyrosine, valine, glutamine or asparagine) at the interior of the β-helix roll (Figure 3, middle panel). Conservative prolines and glycines located at the β-turns also play an important role in the formation and stabilization of the β-helix structure of DcAFP. The C-terminal region of DcAFP (residues 1–47) consists of an 11-residue α-helix, a short α-helix and two short β-strands. The N-terminal region consisting of the final two 3_{10}-helices, the final strand of

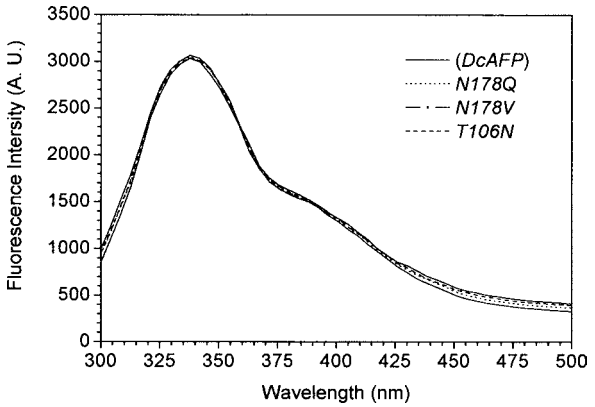

Figure 5 Fluorescence emission spectra of wild-type and mutant DcAFP proteins

Wild-type DcAFP and mutant proteins N178V, N178Q and T106N were detected by fluorescence spectroscopy. All proteins displayed highly similar fluorescence spectra, suggesting that no detectable conformation change was generated in the mutant proteins. Neither blue shift nor red shift of fluorescence emission with a maximum at 338 nm was observed, and all proteins displayed the same emission intensity. A. U., arbitrary units.

sheet B2 and a short loop is stabilized by two disulphide bridges (Cys-275–Cys-297 and Cys-299–Cys-306) (Figure 3, left panel).

The theoretical model of DcAFP shows that a putative ice-binding surface between the two β-sheet rolls (not inside any single β-sheet roll) creates an imperfect complementarity to the 1010 prism plane of ice (Figure 3, right panel). The putative ice-binding surface consists of regularly aligned and strongly conservative asparagines residues in the LRR motif, and their flanking amino acids (79.4 % of which are hydrophilic and 17.1 % are charged), which help to maintain the stability of this ice-binding surface by forming a strongly hydrophilic surface (Figure 3, middle panel). Although the putative ice-binding sites of DcAFP lie between the two β-sheet rolls (not inside them, as is the case in ryegrass and insect AFPs), the inter-residue spacing is similar, i.e. $\sim$4.5 Å between adjacent β-strands and 7.4 Å between residues separated by two positions on the same β-strand. This residue spacing arrangement is thought to facilitate the binding through a complementary surface match to the 1010 prism plane of ice, which has a structure that repeats every 4.52 Å along the α-axis and every 7.35 Å along the c-axis [10].

Significance of conservative asparagine residues for TH activity

In order to validate the structural model, confirm the significance of conservative asparagines for TH activity and provide further insight into the ice-binding mechanism of DcAFP at the molecular level, we carried out non-polar valine mutagenesis and steric glutamine replacements of conservative asparagines within the predicted ice-binding sites.

Recombinant proteins of all mutants expressed in *E. coli* were refolded and purified using the steps described in the Experimental section. The purity of all purified recombinant proteins was evaluated to be $\sim$99 % (Figure 4), and a yield of approx. 18 mg was obtained from 1 litre of induced culture.

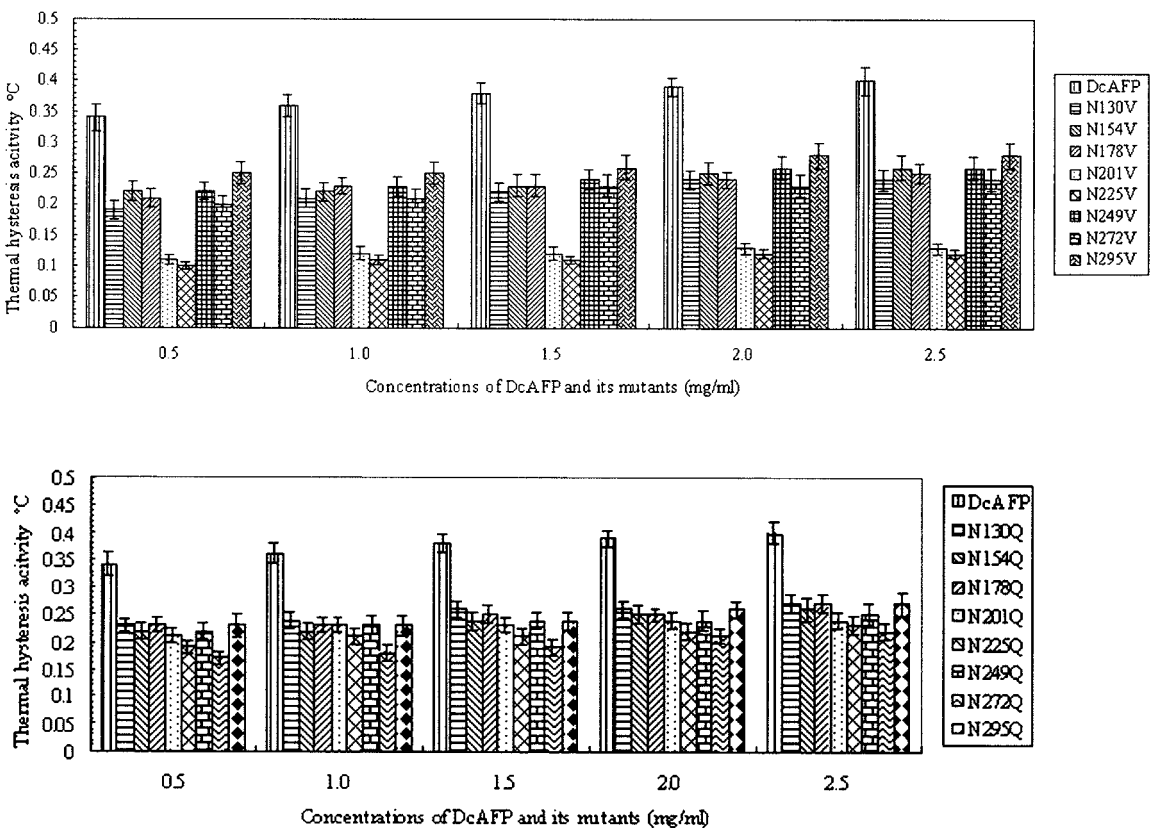

Figure 6 TH activity comparisons between wild-type DcAFP and its Asn → Val (A) and Asn → Gln (B) mutants

TH activity was measured at protein concentrations ranging from 0.5 to 2.5 mg/ml. All mutants displayed a distinct loss of TH activity. This suggests that conserved asparagine residues in the LRR motifs are very important in maintaining the TH activity of DcAFP.

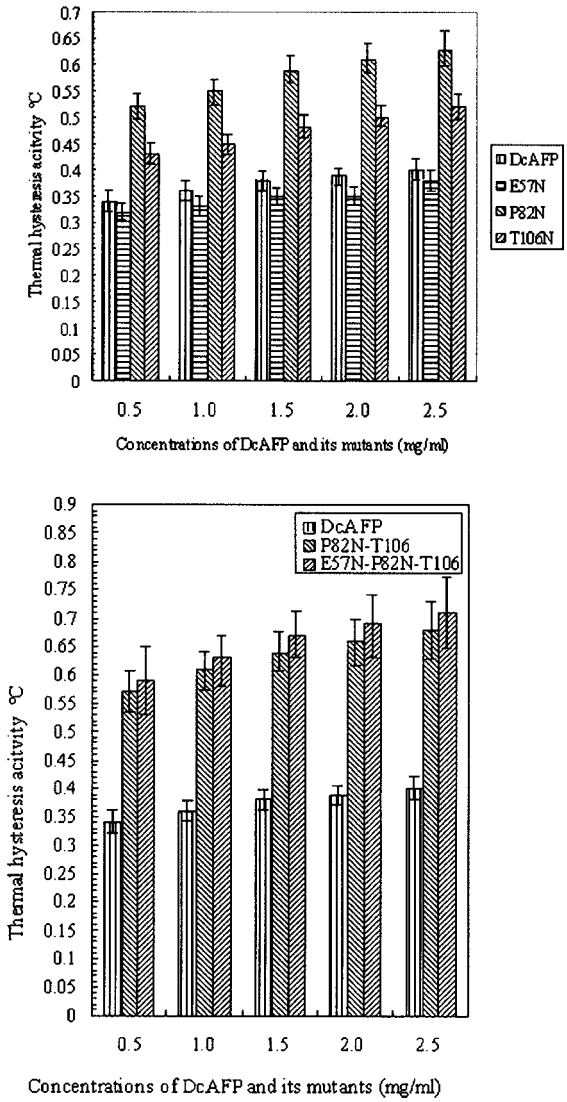

Figure 7 TH activity comparisons between wild-type DcAFP and its asparagine (A) and multi-site (B) mutants

TH activity was measured at protein concentrations ranging from 0.5 to 2.5 mg/ml. The enhanced TH activities of these mutants confirmed that conserved asparagine residues are responsible for the ice-binding sites and the TH activity of DcAFP.

Possible conformational changes of DcAFP mutant proteins expressed in *E. coli* were investigated by fluorescence spectroscopy (Figure 5). The results showed that wild-type DcAFP and its mutants displayed very similar fluorescence spectra; hence it can be concluded that *E. coli*-expressed DcAFP mutants folded well, and that detectable conformational changes were not generated. This suggested that the mutated residues are responsible for the changes in TH activity observed for the DcAFP mutants.

The DcAFP mutants showed differing decreases in TH activity. Mutants N130V, N154V, N178V, N249V, N272V and N295V lowered TH activity by 43%, 37%, 39%, 36%, 41% and 28% respectively, while the N201V and N225V mutants caused a substantial (69% and 71%, respectively) loss of TH activity (Figure 6, upper panel). Steric replacement of conservative asparagines with glutamines also led to distinct decreases in TH activity (Figure 6, lower panel). Mutants N130Q, N154Q, N178Q, N201Q, N225Q, N249Q, N272Q and N295Q lowered TH activity by 32%, 35%, 33%, 39%, 42%, 36%, 50% and 32% respectively.

The above results impelled us to individually replace residues Glu-57, Pro-82 and Thr-106 with asparagine, which will putatively result in the formation of an ice-binding site. Mutant E57N showed a 7% decrease in TH activity, whereas the TH activity of mutants P82N and T106N was increased by 52% and 28% respectively (Figure 7, upper panel). It is suggested that the TH activity would be improved if there were more asparagine residues on the ice-binding site, hence increasing the size of the ice-binding surface.

In order to validate this speculation, multi-site mutation was carried out to obtain mutants P82N/T106N and E57N/P82N/T106N from mutants E57N, P82N and T106N. The TH activity of the two multi-site mutants was increased by 69% and 72% respectively (Figure 7, lower panel). The increment in the TH value of each multi-site mutant was almost equal to the sum of those of each individual mutant. However, there was not a simple linear relationship between the TH activity of the mutants and the size of the ice-binding surface. The overall stability of the β-helix of DcAFP has to be maintained by the helix itself, which has no additional stabilization interaction with other parts of the overall structure, as is seen in many other proteins. In view of the regularity of the ice lattice, too much flexibility on the part of AFP might have detrimental effects on the AFP–ice interaction. Therefore TH activity will be defined by a delicate balance between the ice-binding area and structural flexibility.

DISCUSSION

There is an essential difference between our model of DcAFP and the structure of insect AFPs, although they have similar β-helix structures. The structure of beetle (*Tenebrio molitor*) AFP is stabilized by numerous disulphide and hydrogen bonds, not by a hydrophobic core [10]. The protein fold of spruce budworm (*Choristoneura fumiferana*) AFP is stabilized by numerous disulphide bonds, parallel β-sheets and a weak hydrophobic core [9]. In contrast, the fold of our theoretically modelled DcAFP is supported almost entirely by a strongly hydrophobic core. A common characteristic of insect AFPs is that perfect surface complementarity exists between the AFP and ice. In contrast, the theoretical model of DcAFP shows only imperfect surface complementarity with ice, which may explain the 10–100-fold difference in TH activity between insect and plant AFPs. This imperfect surface complementarity will lead to a distinct weakening of binding to the ice surface, and consequently to a decrease in TH activity. Site-directed mutagenesis of fish and insect AFPs has shown a distinct loss of TH activity when conservative residues in the ice-binding sites were replaced [9,53–55]. The most likely reason for this fall in TH activity is that residue substitutions reduce complementarity with the ice surface, and hence the strength of the interaction, providing a parallel to the weakened binding between DcAFP and ice. The relative weakness of plant AFP TH activity may relate to the freezing tolerance strategy employed by plants. There is no advantage in the plant remaining unfrozen under freezing conditions if there is no environmental liquid water present to maintain normal physiological functions, yet supercooling should be avoided because it would ultimately lead to the rapid, uncontrolled growth of ice [56]. The observed discordance in the effects of plant AFPs on RI and TH, together with an inability to examine the AFP–ice interaction directly, has complicated the direct study of this process.

The enhanced TH activity of P82N and T10N and multi-site mutants P82N/T106N and E57N/P82N/T106N suggests that the

size of the ice-binding face of DcAFP is an important determinant of its antifreeze activity. This finding parallels the observation that a longer isoform of the α-helical fish type I AFP, containing four ice-binding repeats compared with the usual three, was found to be a more potent AFP [57]. A correlation between AFP length and activity has also been described for the AFGPs (antifreeze glycoproteins). Evaluation of the TH activity of various molecular mass isoforms of AFGPs showed that a lower molecular mass, and not amino acid composition, was responsible for the reduced activity of smaller AFGPs [58].

The LRR motif present in DcAFP is also found in PGIPs, ribonuclease inhibitor proteins, cell adhesion factors and blood clotting factors [59]. The common characteristic of proteins with LRR motifs is that they have similar β-helical structures that confer the ability to bind other macromolecules, such as polygalacturonase, ribonuclease and even the surface of ice [60]. It is likely that the different residues exposed on the external faces of each β-helix decide the various binding affinities and abilities.

In summary, DcAFP has highest sequence similarity to PGIP among LRR proteins [3], so the solved crystal structure of PvPGIP was used to perform homology modelling of DcAFP. Our results also indirectly support the theory that DcAFP evolved from LRR-containing proteins, especially PGIP.

This research was supported by the Foundation of National Plant Transgenic Program (J00-A-009) and Natural Science Foundation of Guangdong Province (990258), China.

REFERENCES

1 Urrutia, M. E., Duman, J. G. and Knight, C. A. (1992) Plant thermal hysteresis proteins. Biochim. Biophys. Acta **1121**, 199–206
2 Antikainen, M. and Griffith, M. (1997) Antifreeze protein accumulation in freezing tolerant cereals. Physiol. Plant. **99**, 365–372
3 Worrall, D., Elias, L., Ashford, D., Smallwood, M., Sidebottom, C., Lillford, P., Telford, J., Holt, C. and Bowles, D. (1998) A carrot leucine-rich repeat protein that inhibits ice recrystallization. Science **282**, 11–13
4 Sidebottom, C., Buckley, S., Pudney, P., Twing, S., Jarman, C., Holt, C., Telford, J., McArthur, A., Worrall, D., Hubbard, R. and Lifford, P. (2000) Heat-stable antifreeze protein from grass. Nature (London) **406**, 256
5 Sicheri, F. and Yang, D. S. (1995) Ice-binding structure and mechanism of an antifreeze protein from winter flounder. Nature (London) **375**, 427–431
6 Yeh, Y. and Feeney, R. E. (1996) Antifreeze proteins: Structure and mechanisms of function. Chem. Rev. **96**, 601–617
7 Gronwald, W., Loewen, M. C., Lix, B., Daugulis, A. J., Sonnichsen, F. D., Davies, P. L. and Sykes, B. D. (1998) The solution structure of type II antifreeze protein reveals a new member of the lectin family. Biochemistry **37**, 4712–4721
8 Jia, Z., DeLuca, C. I., Chao, H. and Davies, P. L. (1996) Structural basis for the binding of a globular antifreeze protein to ice. Nature (London) **384**, 285–288
9 Graether, S. P., Kuiper, M. J., Gagne, S. M., Walker, V. K., Jia, Z., Sykes, B. D. and Davies, P. L. (2000) Beta-helix structure and ice-binding properties of a hyperactive antifreeze protein from an insect. Nature (London) **406**, 325–328
10 Liou, Y. C., Tocilj, A., Davies, P. L. and Jia, Z. (2000) Mimicry of ice structure by surface hydroxyls and water of a beta-helix antifreeze protein. Nature (London) **406**, 322–324
11 Kuiper, M. J., Davies, P. L. and Walker, V. K. (2001) A theoretical model of a plant antifreeze protein from *Lolium perenne*. Biophys. J. **81**, 3560–3565
12 Knight, C. A., Cheng, C. C. and DeVries, A. L. (1991) Adsorption of alpha-helical antifreeze peptides on specific ice crystal surface planes. Biophys. J. **59**, 409–418
13 Knight, C. A., Driggers, E. and DeVries, A. L. (1993) Adsorption to ice of fish antifreeze glycopeptides 7 and 8. Biophys. J. **64**, 252–259
14 Knight, C. A. and DeVries, A. L. (1994) Effects of a polymeric, nonequilibrium 'antifreeze' upon ice growth from water. J. Cryst. Growth **143**, 301–310
15 Daley, M. E., Spyracopoulos, L., Jia, Z., Davies, P. L. and Sykes, B. D. (2002) Structure and dynamics of a beta-helical antifreeze protein. Biochemistry **41**, 5515–5525
16 Leinala, E. K., Davies, P. L., Doucet, D., Tyshenko, M. G., Walker, V. K. and Jia, Z. (2002) A beta-helical antifreeze protein isoform with increased activity. Structural and functional insights. J. Biol. Chem. **277**, 33349–33352
17 Cheng, Y., Yang, Z., Tan, H., Liu, R., Chen, G. and Jia, Z. (2002) Analysis of ice-binding sites in fish type II antifreeze protein by quantum mechanics. Biophys. J. **83**, 2202–2210
18 Davies, P. L., Baardsnes, J., Kuiper, M. J. and Walker, V. K. (2002) Structure and function of antifreeze proteins. Philos. Trans. R. Soc. London B **357**, 927–935
19 Achenbach, J. C. and Ewart, K. V. (2002) Structural and functional characterization of a C-type lectin-like antifreeze protein from rainbow smelt (*Osmerus mordax*). Eur. J. Biochem. **269**, 1219–1226
20 Jia, Z. and Davies, P. L. (2002) Antifreeze proteins: an unusual receptor-ligand interaction. Trends Biochem. Sci. **27**, 101–106
21 Leinala, E. K., Davies, P. L. and Jia, Z. (2002) Crystal structure of beta-helical antifreeze protein points to a general ice-binding model. Structure **10**, 619–627
22 Meyer, K., Keil, M. and Naldrett, M. J. (1999) A leucine-rich repeat protein of carrot that exhibits antifreeze activity. FEBS Lett. **447**, 171–178
23 Smallwood, M., Worrall, D., Byass, L., Elias, L., Ashford, D., Doucet, C. J., Holt, C., Telford, J., Lillford, P. and Bowles, D. J. (1999) Isolation and characterization of a novel antifreeze protein from carrot (*Daucus carota*). Biochem. J. **340**, 385–391
24 Fan, Y., Liu, B., Wang, H. B., Wang, S. Q. and Wang, J. F. (2002) Cloning of an antifreeze protein gene in carrot and influence on freeze tolerance of transgenic tobaccos. Plant Cell Rep. **21**, 296–301
25 Knight, C. A., Hallett, J. and DeVries, A. L. (1988) Solute effects on ice recrystallization: an assessment technique. Cryobiology **25**, 55–60
26 Huang, T. and Duman, J. G. (2002) Cloning and characterization of a thermal hysteresis (antifreeze) protein with DNA-binding activity from winter bittersweet nightshade, *Solanum dulcamara*. Plant Mol. Biol. **48**, 339–350
27 Knight, C. A., DeVries, A. L. and Oolman, L. D. (1984) Fish antifreeze protein and the freezing and recrystallization of ice. Nature (London) **308**, 295–296
28 Bujnicki, J. M., Elofsson, A., Fischer, D. and Rychlewski, L. (2001) Structure prediction Meta Server. Bioinformatics **17**, 750–751
29 Gough, J., Karplus, K., Hughey, R. and Chothia, C. (2001) Assignment of homology to genome sequences using a library of hidden Markov models that represent all proteins of known structure. J. Mol. Biol. **313**, 903–919
30 Rychlewski, L., Jaroszewski, L., Li, W. and Godzik, A. (2000) Comparison of sequence profiles. Strategies for structural predictions using sequence information. Protein Sci. **9**, 232–241
31 Kelley, L. A., McCallum, C. M. and Sternberg, M. J. (2000) Enhanced genome annotation using structural profiles in the program 3D-PSSM. J. Mol. Biol. **299**, 499–520
32 Fischer, D. (2000) Hybrid fold recognition: combining sequence derived properties with evolutionary information. Pac. Symp. Biocomput. 2000, 119–130
33 Jones, D. T. (1999) GenTHREADER: an efficient and reliable protein fold recognition method for genomic sequences. J. Mol. Biol. **287**, 797–815
34 Karplus, K., Barrett, C., Cline, M., Diekhans, M., Grate, L. and Hughey, R. (1999) Predicting protein structure using only sequence information. Proteins Suppl. **3**, 121–125
35 Shi, J., Blundell, T. L. and Mizuguchi, K. (2001) Fugue: sequence-structure homology recognition using environment-specific substitution tables and structure-dependent gap penalties. J. Mol. Biol. **310**, 243–257
36 Combet, C., Jambon, M., Deléage, G. and Geourjon, C. (2002) Automatic comparative molecular modelling of protein. Bioinformatics **18**, 213–214
37 Bates, P. A. and Sternberg, M. J. E. (1999) Model building by comparison at CASP3: using expert knowledge and computer automation. Proteins Suppl. **3**, 47–54
38 Cuff, J. A., Clamp, M. E., Siddiqui, A. S., Finlay, M. and Barton, G. J. (1998) JPred: a consensus secondary structure prediction server. Bioinformatics **14**, 892–893
39 Rost, B. (1996) PHD: predicting one-dimensional protein structure by profile based neural networks. Methods Enzymol. **266**, 525–539
40 Carey, M. J., DeWitt, D. J., Naughton, J. F., Asgarian, M., Gehrke, J. E. and Shah, D. N. (1997) The BUCKY object-relational benchmark. In Proceedings of the 1997 SIGMOD Conference, May 18, 1997, Tucson, AZ
41 McGuffin, L. J., Bryson, K. and Jones, D. T. (2000) The PSIPRED protein structure prediction server. Bioinformatics **16**, 404–405
42 Lundstrom, J., Rychlewski, L., Bujnicki, J. M. and Elofsson, A. (2001) A neural-network-based consensus predictor that improves fold recognition. Protein Sci. **10**, 2354–2362
43 Guex, N. and Peitsch, M. C. (1997) SWISS-MODEL and the Swiss-PDB Viewer: an environment for comparative protein modeling. Electrophoresis **18**, 2714–2723
44 Luthy, R., Bowie, J. U. and Eisenberg, D. (1992) Assessment of protein models with three-dimensional profiles. Nature (London) **356**, 83–85
45 Martz, E. (2002) Protein explorer: easy yet powerful macromolecular visualization. Trends Biochem. Sci. **27**, 107–109
46 Aloy, P., Moont, G., Gabb, H. A., Querol, E., Aviles, F. X. and Sternberg, M. J. E. (1998) Modelling protein docking using shape complimentarity, electrostatics and biochemical information. Proteins **33**, 535–549
47 Ho, S. N., Hunt, H. D., Horton, R. M., Pllen, J. K. and Pease, L. R. (1988) Site-directed mutagenesis by overlap extension using the polymerase chain reaction. Gene **77**, 61–68

48 Studier, F. W., Rosenberg, A. H., Dunn, J. J. and Dubendorff, J. W. (1990) Use of T7 RNA polymerase to direct expression of cloned genes. Methods Enzymol. **185**, 60–89
49 Burgess, R. R. (1996) Purification of overproduced Escherichia coli RNA polymerase sigma factors by solubilizing inclusion bodies and refolding from sarkosyl. Methods Enzymol. **273**, 145–149
50 Zhang, D. Q., Liu, B., Fang, Y., He, Y. M. and Wang, J. F. (2003) High efficient expression of carrot antifreeze protein in E. coli. Zhongshan Daxue Xuebao, Ziran Kexueban **42**, 51–55
51 Chakrabartty, A. and Hew, C. L. (1991) The effect of enhanced alpha-helicity on the activity of a winter flounder antifreeze polypeptide. Eur. J. Biochem. **202**, 1057–1063
52 Di Matteo, A., Federici, L., Mattei B., Salvi, G., Johnson, K. A., Savino, C., De Lorenzo, G., Tsernoglou, D. and Cervone, F. (2003) The crystal structure of polygalacturonase-inhibiting protein (PGIP), a leucine-rich repeat protein involved in plant defense. Proc. Natl. Acad. Sci. U.S.A. **100**, 10124–10128
53 Chao, H., Houston, M. E. J., Hodges, R. S., Kay, C. M., Sykes, B. D., Loewen, M. C., Davies, P. L. and Sönnichsen, F. D. (1997) A diminished role for hydrogen bonds in antifreeze protein binding to ice. Biochemistry **36**, 14652–14660
54 Haymet, A. D., Ward, L. G., Harding, M. M. and Knight, C. A. (1998) Valine substituted winter flounder 'antifreeze': preservation of ice growth hysteresis. FEBS Lett. **430**, 301–306
55 Zhang, W. and Laursen, R. A. (1998) Structure-function relationships in a type I antifreeze polypeptide. The role of threonine methyl and hydroxyl groups in antifreeze activity. J. Biol. Chem. **273**, 34806–34812
56 Duman, J. G. (2001) Antifreeze and ice nucleator proteins in terrestrial arthropods. Annu. Rev. Physiol. **63**, 327–357
57 Chao, H., Hodges, R. S., Kay, C. M., Gauthier, S. Y. and Davies, P. L. (1996) A natural variant of type I antifreeze protein with four ice-binding repeats is a particularly potent antifreeze. Protein Sci. **5**, 1150–1156
58 Schrag, J. D., O'Grady, S. M. and DeVries, A. L. (1982) Relationship of amino acid composition and molecular weight of antifreeze glycopeptides to non-colligative freezing point depression. Biochim. Biophys. Acta **717**, 322–326
59 Kobe, B. and Deisenhofer, J. (1995) A structural basis of the interactions between leucine-rich repeats and protein ligands. Nature (London) **374**, 183–186
60 Jenkinsa, J. and Pickersgill, R. (2001) The architecture of parallel β-helices and related folds. Prog. Biophys. Mol. Biol. **77**, 111–175

Received 15 August 2003/6 October 2003; accepted 8 October 2003
Published as BJ Immediate Publication 8 October 2003, DOI 10.1042/BJ20031249